Blocking-assisted infrared transmission of subwavelength metallic gratings by graphene

Blocking-assisted infrared transmission of subwavelength metallic gratings by graphene

X L Liu, B Zhao and Z M Zhang

George W. Woodruff School of Mechanical Engineering, Georgia Institute of Technology, Atlanta, GA 30332, USA

E-mail: zhuomin.zhang@me.gatech.edu

CrossMark

Abstract

The transmittance of simple one-dimensional gratings and two-dimensional pillar arrays is usually broadband with poor selectivity in the infrared region. In this paper, it is demonstrated that covering graphene on top of a Ag grating will improve both the magnitude and coherence of the transmitted infrared radiation. The underlying mechanism of this anomalous blocking-assisted transmission is attributed to the excitation of localized magnetic resonances. Quantitative predictions of the resonance wavelength for different geometric parameters and graphene chemical potentials are provided based on the equivalent-circuit model. The enhancement is alignment-free and actively tunable. Such graphene-covered gratings may help improve the performance and robustness of optical devices, such as polarizers, color filters, lab-on-chip sensors, and transparent conductors.

Keywords: graphene, anomalous transmission, subwavelength gratings, optical properties

(Some figures may appear in colour only in the online journal)

1. Introduction

Metallic films are commonly used as high-reflection coatings in many optical systems due to the substantial mismatch of impedance induced by the high density of free electrons. For example, depositing thin metal coatings on glass to make mirrors began as early as the 19th century. In stark contrast to opaque metallic films, perforated films might support extraordinary optical transmission (EOT) with efficiencies that are orders of magnitude beyond geometry-based classic theory. This interesting EOT phenomenon has received extensive attention since the seminal work [1]. Both one-dimensional (1D) and two-dimensional (2D) slit arrays have been investigated from the visible to the microwave regions [2–12]. The wide applications of EOT in optical devices include but are not limited to high-contrast polarizers or modulator [13], color filters [14], and transparent conductors [15]. EOT has also been used for designing lab-on-chip sensors due to the highly localized sensing area and simpler optical setup compared with typical Kretschmann-configuration-based sensing

[16–18]. Double-layer slit arrays separated by a thin dielectric film [19–23] have also been intensively investigated. The transmission performance could be improved in certain wavelength region but it is very sensitive to the alignment between the two layers and thickness of the dielectric film, making the fabrication quite challenging and thus hindering practical applications. The transmission of simple metallic 1D gratings and 2D pillar arrays is broadband in the low-frequency region since no resonances are excited. However, this property impedes the above nanostructures to be used as sensors or color filters in long wavelengths although extraordinary transmission is supported.

Graphene, a 2D layered material with carbon atoms arranged in a honeycomb lattice, exhibits metallic behavior when chemical doping or electric gating is applied [24–26]. This 2D Dirac material supports unprecedented optical properties beyond conventional metals such as extreme light confinement, low loss, high carrier mobility and tunable graphene plasmon frequency ranging from near-infrared to terahertz [27]. The present paper theoretically demonstrates
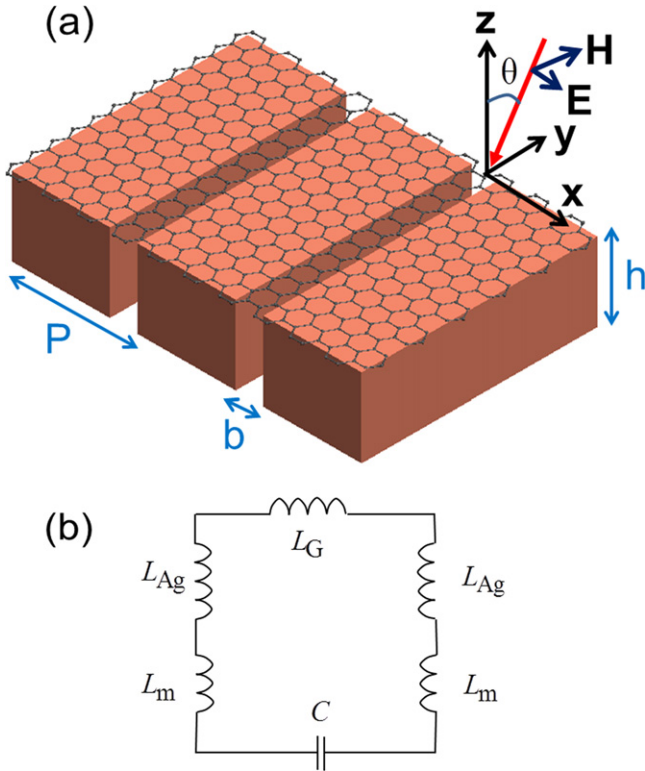
Figure 1. (a) Schematic of graphene-coated 1D Ag grating. Only TM wave is considered. Note that θ is the incidence angle, P the period, b the slit width and h the grating height; (b) LC model for prediction of the resonance wavelength.

that it is possible to achieve resonance transmission of simple 1D gratings and 2D pillar arrays in the infrared wavelength region by depositing monoatomic layer of graphene. The blockage of this 2D conductive film can counterintuitively enhance the transmission performance.

2. Method and analysis

Consider a graphene-covered 1D Ag grating as shown in figure 1(a). The grating or slit array is periodic along the x direction and extends to infinity in the y direction with a period P, height h, and slit width b. The incidence angle is θ, and thus the incident wavevector can be written as $(-k_0 \sin \theta, 0, -k_0 \sin \theta)$ with k_0 being the wavevector in the free space. Only transverse magnetic (TM) waves with magnetic field along the y direction are considered since the transmittance for transverse electric (TE) wave is essentially zero for 1D grating. In the mid-infrared wavelength region, the optical response of 1D metal grating to TE waves can be approximated by a diluted Drude model weighted by the volume filling ratio [28], and this metallic response precludes the transmission of TE waves. Optical conductivity of graphene σ, which includes both interband and intraband (Drude-like) contributions, depends on the chemical potential μ, electron relaxation time τ, and temperature T, and is given as

[29, 30].

$$\sigma = \sigma_{\text{Inter}}(\omega, \mu, T) + \sigma_{\text{Drude}}(\omega, \mu, T), \qquad (1)$$

$$\sigma_{\text{Inter}} = \frac{e^2}{4\hbar} \left[G\left(\frac{\hbar\omega}{2} \right) + \mathrm{i}\frac{4\hbar\omega}{\pi} \right.$$
$$\left. \times \int_{\eta=0}^{\infty} \frac{G(\eta) - G(\hbar\omega/2)}{(\hbar\omega)^2 - 4\eta^2} d\eta \right], \qquad (2)$$

$$\sigma_{\text{Drude}} = \frac{\mathrm{i}}{\omega + \mathrm{i}/\tau} \frac{e^2}{\pi\hbar^2} 2k_{\text{B}}T \ln \left[2 \cosh\left(\frac{\mu}{2k_{\text{B}}T} \right) \right], \qquad (3)$$

where
$G(\eta) = \sinh(\eta/k_{\text{B}}T) / \left[\cosh(\eta/k_{\text{B}}T) + \cosh(\mu/k_{\text{B}}T) \right]$. The graphene conductivity used in this work is calculated by setting $\tau = 10^{-13}$ s and temperature $T = 300$ K. The chemical potential μ can be tuned by chemical doping or electrostatic gating. The dielectric function of Ag is obtained using a simple Drude model: $\varepsilon_{\text{Ag}} = 1 - \omega_p^2 / (\omega^2 + \mathrm{i}\gamma\omega)$ with a scattering rate $\gamma = 2.73 \times 10^{13}$ rad s^{-1} and plasma frequency $\omega_p = 1.37 \times 10^{16}$ rad s^{-1} [31].

The computation for 1D grating is based on the rigorous coupled-wave analysis (RCWA) algorithm [19, 31]. This is a semi-analytical method based on Fourier space expansion. The light shines on the nanostructures and then is diffracted into infinite orders by the periodic structure. Practically, the series expansion should be truncated by sufficient order N [31]. The tangential wavevector of different orders of diffracted light is governed by the Bloch–Floquet condition [32]. The harmonic coefficients of different orders can then be obtained by applying the boundary conditions that the tangential fields should be continuous across the interface. The code employed is home-made and has been released to public [33]. The electromagnetic response of 2D graphene can be described by a surface current $J = \sigma E_{\text{t}}$, where E_{t} is the tangential field parallel to x–y plane. For graphene-covered gratings, the reflection coefficient for any order can be obtained by considering that tangential magnetic fields are mediated by the surface current due to the addition of the graphene layer [34]. Alternatively, graphene can be treated as an atomically thin film with isotropic optical response whose dielectric function is given by $\varepsilon_{\text{G}} = 1 + \mathrm{i}\sigma / (\omega\Delta\varepsilon_0)$ [35], where Δ is the effective thickness, ε_0 is the permittivity of vacuum. Both methods yield almost identical transmittance as long as Δ is smaller than 0.5 nm. The diffraction order N used in this study is 300, which is high enough to accurately predict the radiative properties. For field plots, higher orders are used to ensure convergence. The analysis of 2D grating is based on finite-difference time-domain (FDTD) method using a commercial package (Lumerical Solutions) since it is difficult to obtain convergent results with 2D RCWA [32].

Besides RCWA and FDTD methods, equivalent circuit models are employed to help elucidate the underlying mechanism for the blocking-enhanced transmission. Inductor–capacitor (LC) circuit model, initially introduced to analyze the electromagnetic properties of split-ring resonators [36, 37], has been widely used to predict the resonances of

more general metamaterials such as 1D and 2D gratings [13, 38–43]. The LC model corresponding to figure 1(a) can be described as in figure 1(b). The air inside the slit acts as a dielectric capacitor with a capacitance of $C = \varepsilon_0 hl/b$, where l is a prescribed length in the y direction. The Ag walls around the slit and graphene serve as conductors, and their kinetic inductances are determined by [13, 38].

$$L_{\mathrm{Ag}} = -\frac{h}{\varepsilon_0 \omega^2 l \delta} \frac{\varepsilon'_{\mathrm{Ag}}}{\left(\varepsilon'^2_{\mathrm{Ag}} + \varepsilon''^2_{\mathrm{Ag}} \right)}, \qquad (4)$$

$$L_{\mathrm{G}} = \frac{c_1 b}{\omega l} \frac{\sigma''}{\left(\sigma'^2 + \sigma''^2 \right)}, \qquad (5)$$

where δ is the penetration depth expressed as $\lambda/(4\pi\kappa)$ that takes into account the effective cross-section area for the induced current. Note that λ is the wavelength in vacuum and κ is the extinction coefficient of Ag. Coefficient c_1 is introduced because the length of graphene involved in the resonance is longer than the slit width due to the finite cross-section width of current in the slit wall. It could be affected by the slit width or period; however, $c_1 = 1.3$ is chosen in the present study as a reasonable representative value. The mutual inductance is given as $L_m = \mu_0 hb/2l$ [38, 39], where μ_0 is the permeability of vacuum. This LC model can be confirmed by the distribution of current density shown in the next section. By zeroing the total impedance $i\omega\left(2L_{\mathrm{Ag}} + L_{\mathrm{G}} + 2L_m - \omega^{-2}C^{-1} \right)$, the resonance wavelength of magnetic polariton (MP) can be obtained as

$$\lambda_{\mathrm{MP}} = 2\pi c_0 \sqrt{\left(2L_{\mathrm{Ag}} + L_{\mathrm{G}} + 2L_m \right)C}, \qquad (6)$$

3. Results and discussion

Figure 2(a) gives the transmittance for plain and graphene-coated grating at normal incidence with $P = 1000$ nm, $b = 50$ nm, $h = 200$ nm, and $\mu = 0.8$ eV. The transmittance of plain grating is much greater than the filling ratio of the slit area 0.05 and monochromatically increases with wavelength. Nevertheless, the transmission selectivity is too poor to make 1D grating available as color filters or sensors in the long wavelength. When the wavelength is much longer than the period, according to effective medium theory [28, 44, 45], 1D and 2D nanopillars can be homogenized as uniaxial materials with optical axis lying tangentially and longitudinally, respectively. At normal incidence, the wavevector in the longitudinal direction (z axis) depends only on the effective dielectric function in the tangential direction. For both 1D nanopillars (only for TM waves) [28] and 2D nanopillars [44, 45], the imaginary part of this effective dielectric function approaches to zero especially with increasing wavelengths. That is because at low frequencies (long wavelengths), Ag acts like a perfect conductor with diminishing electric fields inside. Thus the electric field is nontrivial only in the slit region. Then nanopillars behave as a dielectric with low loss and a finite thickness, as a result, the
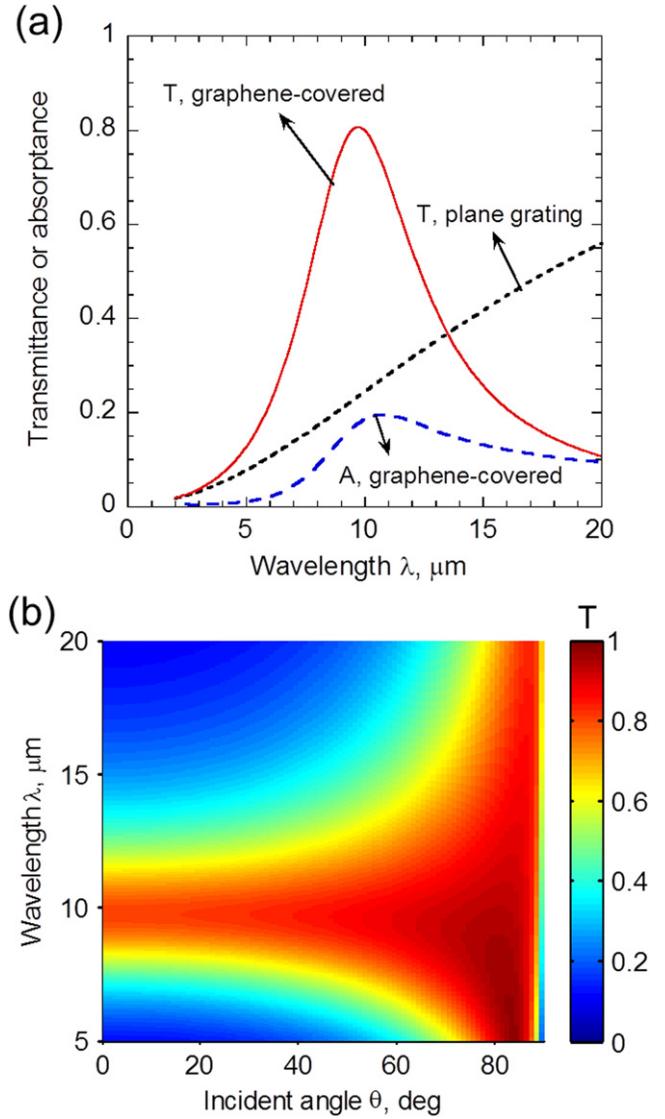

Figure 2. (a) Normal transmittance and absorptance spectra for plain and graphene-covered gratings; (b) contour plot of the transmittance as a function of wavelength and incidence angle. The parameters are $P = 1\ \mu$m, $b = 50$ nm, $h = 200$ nm, $\mu = 0.8$ eV.

transmittance of plain grating is high, and tends to further increase with wavelength. After depositing atomic thin graphene layer, a resonance transmission is clearly shown with a peak near $\lambda = 10\ \mu$m. A transmission preference occurs in contrast to the previous incoherent transmittance. For wavelengths ranging from 5 to 13.5 μm, covering the Ag grating with graphene improves its transparency. The maximum transmittance reaches 0.81 at $\lambda = 9.72\ \mu$m, 3.5 times as high as that of the plain grating. This anomalous improvement is robust and alignment-free compared with using double-layer grating since graphene is a continuous sheet. The reflectance at 9.72 μm (not shown) is reduced substantially from 0.76 to 0.02, leading to an antireflection effect. The absorptance (A) of the plain grating is negligible (not shown) but increases to 0.17 at the resonance after being covered with graphene. Note that the absorptance of free-standing graphene is very low (less than 1%) in the mid-infrared region, suggesting that

gratings can significantly enhance graphene absorption. This might be important for improving the performance of graphene-based optical devices relying on its absorption properties such as ultrafast optoelectronics enabled by the vanishing effective mass of free carriers in graphene. Similar phenomena of enhancing the absorption of graphene have recently been demonstrated in the visible and near-infrared region [46, 47]. Away from the resonance with wavelengths longer than 13.5 μm, coating metallic graphene will deteriorate the transmittance. This is not surprising since doped graphene is essentially a thin metallic film and has a low transmittance in the far-infrared region.

Figure 2(b) displays the transmittance contour of 1D grating, showing the dependence on both the wavelength and incidence angle, while other parameters are the same as those used in figure 2(a). Clearly, the wavelength of the transmission peak is insensitive to the incidence angle; this is a distinct characteristic of MP [13, 32, 40, 42, 48], which will be further confirmed by the field and current density distribution. MP is the strong coupling between the magnetic resonance inside a micro/nanostructure and the external electromagnetic waves. The time-varying magnetic field parallel to the y-direction creates an oscillating current loop in the x–z plane, which generates a localized enhanced electromagnetic field that indicates diamagnetic response [32]. Another interesting feature is the broadband high transmittance close to grazing incidence. This is associated with deep metallic gratings and has been explained previously based on either spoof surface plasmons [49] or impedance matching [50].

The magnetic field and current density vectors near the slit are shown in figure 3(a) to elucidate the underlying mechanism for the anomalous blocking-assisted transmission. The contour is for $\left| H_y/H_0 \right|^2$ and black arrows represent the instantaneous current density vectors. Note that $z = 0$ and $z = -0.2\,\mu$m denote the upper and lower boundaries of the Ag grating, respectively. Large field enhancement exists in the slit region ($-0.025 < x < 0.025\,\mu$m) especially near the graphene, suggesting a localized resonance. High field concentration can also be seen from the contour plots of electric fields as shown in figure 3(b). The relative field amplitude in the incident vacuum region is close to one, suggesting that the reflection is very small. The current density in the graphene is very high and is denoted as the white arrows pointing left. There is a displacement current in the air gap pointing right as indicated in figure 3(a). Combined with the counter-parallel current density vectors in Ag, it can be seen that a closed current loop is formed around the slit region as indicated by the oval, manifesting the existence of a magnetic resonance. The distribution of the current density vectors agrees with the LC model given in figure 1(b), which is thus reasonable to be used for predicting the MP resonance wavelength.

The resonance wavelength predicted by the LC models given in equation (6) is 9.57 μm, which agrees well with 9.72 μm obtained by numerical simulations. The insensitivity of resonance transmission to the incident angle as shown in figure 2(b) can be explained by equation (6) since there are no terms related to θ. Therefore, the transmission peak is due to
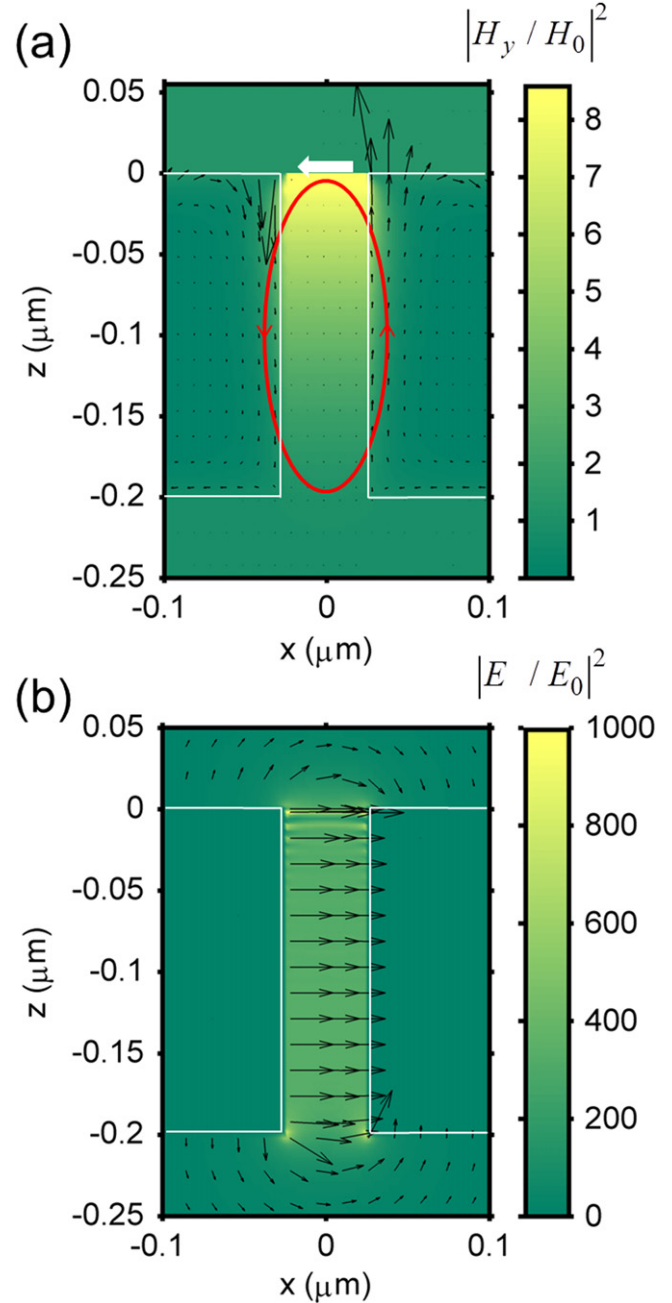

Figure 3. (a) Enhancement of the magnetic field $\left| H_y/H_0 \right|^2$ at 9.72 μm where MP resonance is excited. The black arrows are the current density vectors, the white arrow indicates current flow in the graphene, the oval represents the current loop. (b) Enhancement of the electric field $\left| E/E_0 \right|^2$ with black arrows as the electric field vectors. The white lines are boundaries of Ag grating.

the excitation of MP resonance. This MP resonance is not achievable in the infrared region without the coated single layer graphene sheet, which provides the dominant inductance required for the LC resonance. Strong localized field in the slit region due to resonance excitation helps photons pass through and reduces the reflection [13]. Note that graphene has been demonstrated to tune the resonances of metallic antennas since evanescent waves with large-wavevectors can
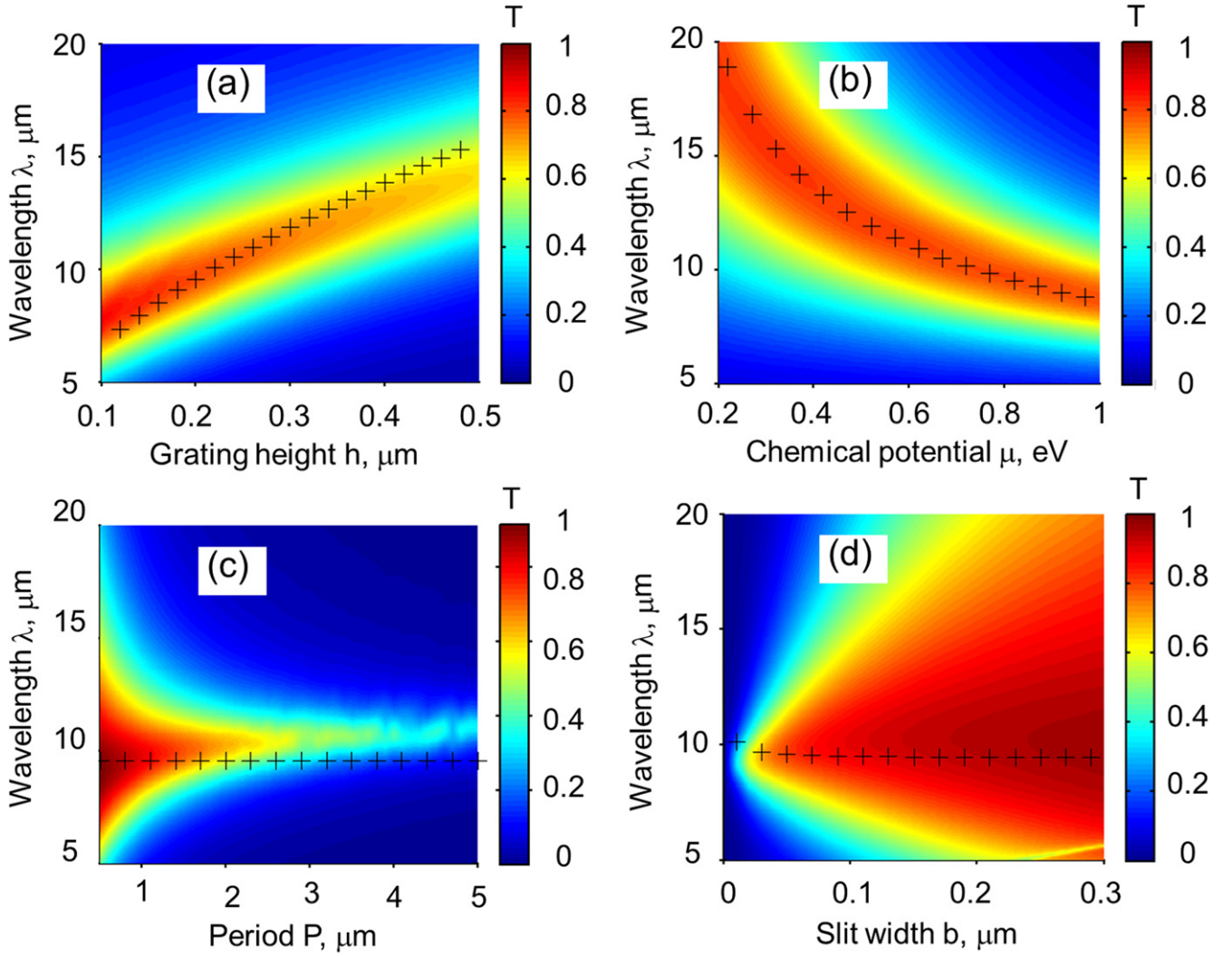
Figure 4. Normal transmittance contours with varying parameters: (a) grating height; (b) chemical potential; (c) period; (d) slit width. Only one parameter is changed in each plot compared with figure 2(a). The + marks indicate the wavelength corresponding to the transmission peak calculated from the LC model using equation (6).

couple with the graphene plasmons [51, 52]. Graphene ribbons or gratings can launch graphene plasmons directly to achieve some resonance effects since the momentum mismatch can be provided by the surface diffraction [53, 54]. The angle-insensitive MP resonance assisted by graphene at low frequencies discussed here is different from the above-mentioned scenarios.

The effects of various geometric parameters and chemical potential of graphene on the transmittance at normal incidence are shown in figure 4 by changing one parameter while maintaining other parameters at the default values as those in figure 2(a). The prediction from the LC model as indicated by the cross mark generally agrees well with that from the RCWA. As shown in figure 4(a), the resonance wavelength monotonically increases with grating height. This trend can be easily predicted by equation (6) since both L_{Ag} and C increase with h. With increasing chemical potential, the number of free electrons in graphene increases, leading to a higher conductivity. Then L_G decreases; according to equation (6), this gives a blueshift of MP resonance as shown

in figure 4(b). With increasing chemical potential, the coherence (Q factor) is improved with smaller full width at half maximum. By employing complex nanopillars with different parameters, such as chemical potentials and grating height, used in neighboring periods [55–57], the transmission can be tuned to be multiband to meet different demands.

Figure 4(c) illustrates the effects of period on the transmittance. The transmission peak is not sensitive to the period, and this can be explained by the LC model since MP is a localized resonance and there are no terms related to the period in equation (6). Similar results were found in [39] for deep gratings without graphene coverage. The bandwidth of the transmittance peak is tunable and becomes narrower at larger P. This phenomenon is desired for filters that allow radiation in certain desired wavelength region to pass. However, the transmission intensity will deteriorate to some extent at large period while keeping the same slit width. Another tunable parameter is the slit width, whose effect is shown in figure 4(d). The transmission peak appears to be insensitive to b and this can also be predicted by the LC model. Note that

the capacitance C is inversely proportional to b while both L_G and L_m are linearly proportional to b. Given that L_{Ag} is small compared with L_G, the resonant wavelength should be almost independent of b according to equation (6). The deviation between the LC model and RCWA simulations may be due to the approximation of c_1, as well as the nonuniform charge distribution that could affect the gap capacitance [35]. Overall, the simple LC model not only provides a physical interpretation of the anomalous transmission, but also allows quantitative understanding of the dependence of the resonance condition on the geometric and materials properties.

The imaginary part of the conductivity of doped graphene is positive, leading to a negative real part of the dielectric permittivity according to the finite-thickness model [35]. Therefore, doped graphene has a metallic characteristic. One might wonder whether the previously discussed blocking-assisted resonance transmission will hold if graphene is replaced by a thin layer of conventional metal film. As shown in figure 5(a), similar anomalous transmittance phenomenon is supported in a narrower band when a Ag film with various thicknesses is deposited on the top side of the grating. Assuming the bulk dielectric function applies to thin Ag film without considering the increased scattering rates due to electron collisions with boundaries, the peak transmission calculated using RCWA occurs at $\lambda = 3.54\,\mu m$ for a thickness of 0.5 nm as shown in figure 5(a). This is in good agreement with the value of 3.76 μm predicted by equation (6) where L_G becomes $-\frac{c_1 b}{\varepsilon_0 \omega^2 l d}\left(\frac{\varepsilon'_{Ag}}{\varepsilon'^2_{Ag} + \varepsilon''^2_{Ag}}\right)$, where d is the thickness of the Ag film. The agreement in the resonance wavelength between LC model and exact numerical method holds for different film thicknesses as shown in figure 5(b). Decreasing Ag film thickness will redshift and broaden the transmission as shown in figure 5(a), which is similar to the effect of decreasing graphene chemical potential as shown in figure 4(b). This is due to the increased kinetic inductance of Ag film. Increasing Ag thickness will have the opposite effect. The transmission peak can be easily tuned by controlling the thickness of Ag film, but it should be noted that fabrication of a uniform suspended Ag film of sub nanometer thickness across the slit region is very challenging with present-day technologies. Therefore, doped graphene is advantageous over metallic films in terms of enhancing the transmission magnitude and coherence of gratings or slit arrays since its fabrication and transfer techniques have been successfully demonstrated.

Covering graphene on both sides of the Ag grating can lead to similar resonance transmission as shown in figure 6(a) for different chemical potentials at normal incidence. The chemical potential is assumed to be the same for both the top and bottom graphene. The resonance wavelength increases with decreasing chemical potential, which has the same trend as figure 4(b). The field plot for $\mu = 0.8\,eV$ at resonance wavelength of 6.87 μm is given in figure 6(b), which clearly shows that there are two split localized resonances excited near the bottom and top graphene sheet respectively. As indicated by the arrows, two identical current loops but with opposite directions are supported. The LC model in figure 1(b) and equation (6) can be used directly to predict the
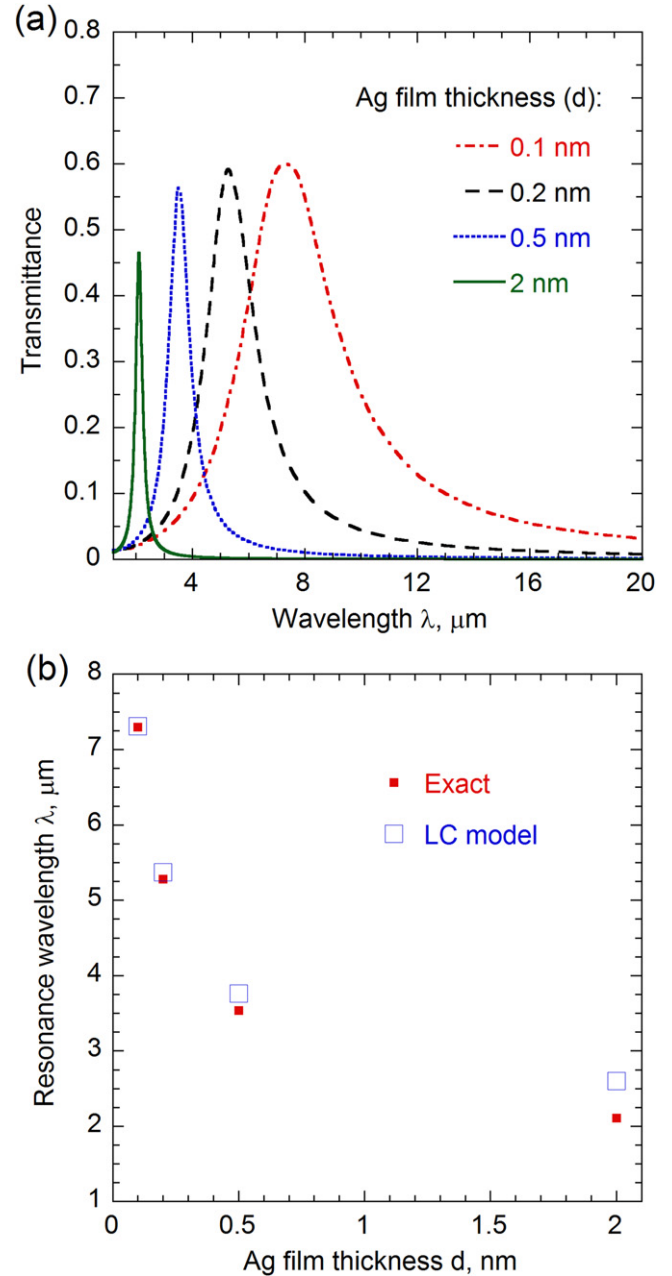

Figure 5. (a) Transmittance spectra when covering a thin Ag film of various thicknesses on top of the Ag grating; (b) the resonance wavelength versus film thickness obtained by using exact method and LC model.

resonance position considering that half of the total grating height should be used. The resonance peak is then predicted to be 6.68 μm. This agrees with the peak location occurring at $\lambda = 6.87\,\mu m$ obtained by using RCWA as shown in figure 6(a). The peak transmittance is still around 80%, but the resonance wavelength decreases by approximately $\sqrt{2}$ from 9.72 μm to 6.87 μm after covering graphene on both sides. This is because the capacitance is reduced by 50% while the total kinetic inductance barely changes due to the dominant contribution of graphene, whose inductance is independent of the grating height. These examples not only help further demonstrate the validity of the LC model and
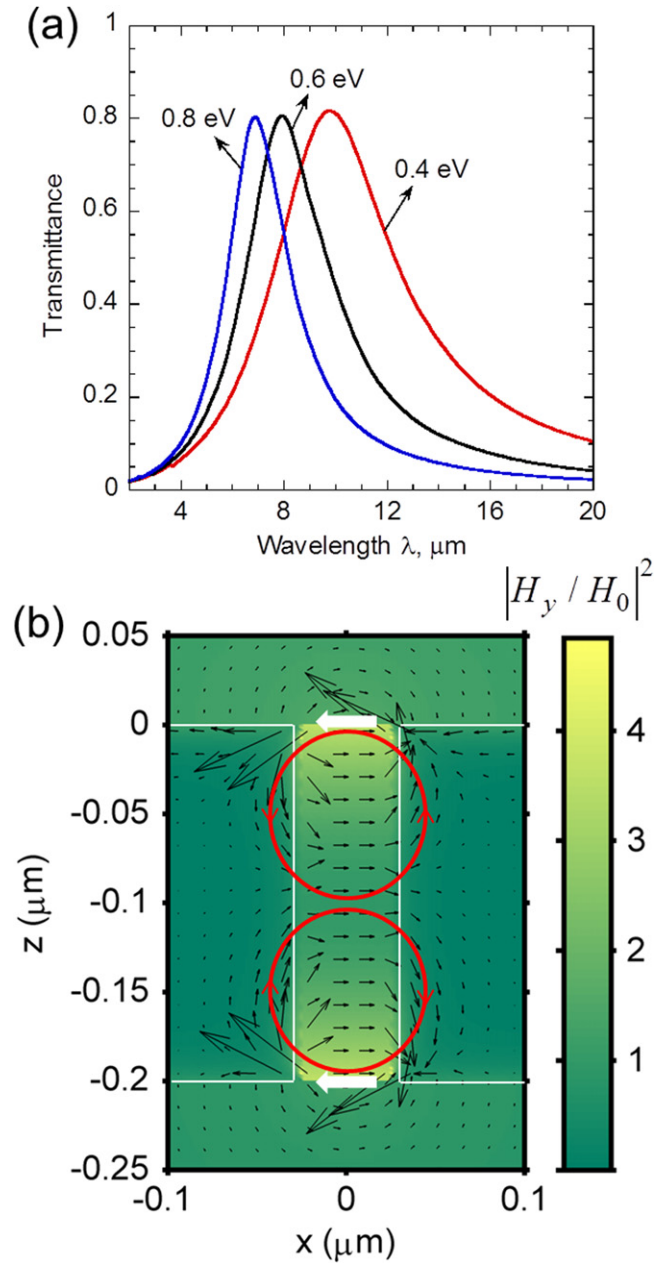
Figure 6. (a) Transmittance spectra for Ag grating with graphene coverage on both sides; (b) magnetic field at resonance peak of 6.87 μm. Circles show the two current loops with opposite directions. The grating geometry and graphene chemical potential are the same as given in figure 2.

Figure 7. (a) Schematic of graphene-covered 2D pillar arrays with periods and slit widths in *x* and *y* directions as P_x, P_y, b_x, b_y. h_2 is the grating height. (b) Transmittance of plain and graphene-covered 2D pillar arrays at normal incidence for different chemical potentials but with geometric parameters as the same as what used in figure 2.

confirm the MP resonance excitation, but also suggest alternative methods for tuning the transmission peaks.

The aforementioned blocking-assisted transmission is supported only by TM waves for 1D grating while the transmittance of TE waves is so small that adding graphene will have negligible effects. As a result, the proposed structure can be used for polarizers with better performance than plain 1D Ag grating. Nevertheless, for some applications such as transparent electrodes, polarization-insensitivity might be desired, otherwise half of the total energy will be lost. This necessitates the analysis of 2D pillars whose schematic is shown in figure 7(a). P_x (b_x) and P_y (b_y) are the period (slit
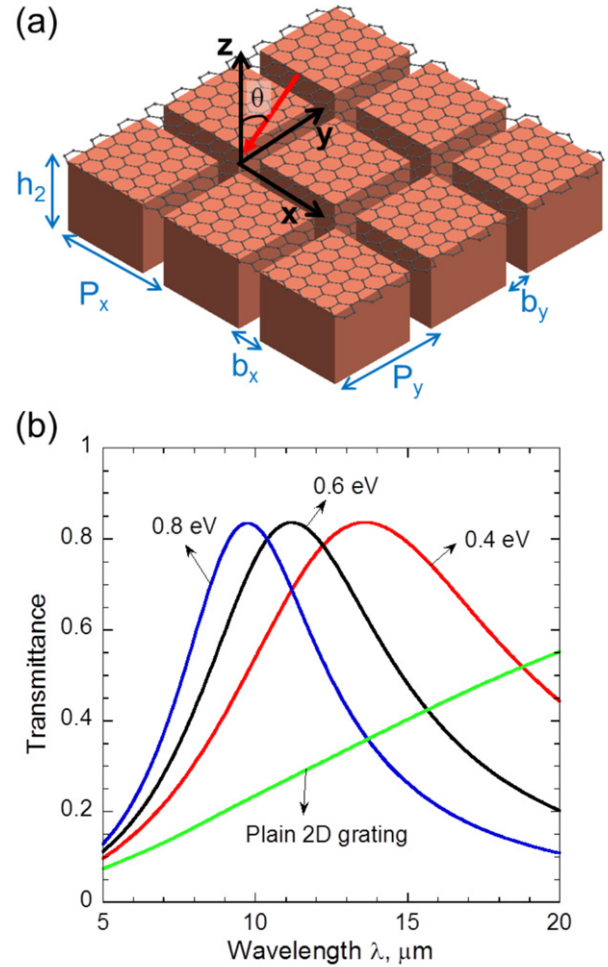
width) in the *x* and *y* directions, respectively, and h_2 is the grating thickness. Figure 7(b) gives the transmission of plain and graphene-covered 2D pillar arrays at normal incidence with $P_x = P_y = 1\,\mu$m, $b_x = b_y = 0.05\,\mu$m, and $h_2 = 0.2\,\mu$m for different values of chemical potentials. Similar anomalous enhanced transmission over plain 2D pillar arrays can be clearly observed by coating a single layer of graphene sheet. The transmission performance of 2D pillar arrays does not change much compared with 1D counterparts at the same geometric parameters and graphene chemical potential. One distinction from 1D grating is that there is no difference between TE and TM waves at normal incidence for 2D pillars due to the structure symmetry. Therefore, graphene-covered 2D metallic grating can be used for transparent electrodes, filters, or sensors with no polarization preference.

Similar blocking-assisted transmission by graphene can be found in subwavelength gratings made of other metals (Au or Al) or doped semiconductors (such as doped silicon) or

polar materials (such as SiC), although the results are not presented here. Depositing graphene or atomically thin metal film on one side or two sides of the grating helps to excite and tune the resonances, whose net effects are not limited to enhancing the transmission and coherence. Meanwhile, the light is concentrated in a small slit region beyond the diffraction limit as can be seen from figure 3 [5]. This might assist the light management of long wavelengths in deep subwavelength scale and enhance matter–wave interactions, such as Raman scattering, spontaneous emission, and non-linear processes, by using simple 1D or 2D gratings. In addition, devices such as polarizers or filters based on the proposed configuration is very thin, only about 2% of the wavelength, and thus can be easily incorporated with other compact optical devices. It can also work independently when mounted on different transparent substrates in the infrared region such as silicon.

4. Conclusions

In summary, covering 1D and 2D Ag gratings with a single-layer graphene is found to counterintuitively increase the transmission several fold in certain wavelength region. Transmission preference can be obtained by exciting resonances which are not available in the long wavelength for simple 1D and 2D gratings. The enhancement is robust and alignment-free, and can be actively tuned by changing the chemical potential of graphene through electric gating. Coating graphene on both sides of the Ag grating provides another way to tune the resonance transmission. The anomalous blocking-assisted transmission is attributed to the excitation of MP, a localized resonance. A simple LC model is presented to quantitatively predict the wavelength of the transmittance peak for different geometric parameters and graphene chemical potentials. Replacing graphene by atomically thin metallic film will have similar effects though the fabrication is formidable. Covering graphene helps to enhance the transparency, improve the transmission coherence, and light confinement in nanoslits. This work may be used to enhance the performance of polarizers, transparent conductors, and infrared filters.

Acknowledgments

References

[1] Ebbesen T W, Lezec H J, Ghaemi H F, Thio T and Wolff P A 1998 Extraordinary optical transmission through sub-wavelength hole arrays *Nature* **391** 667–9

[2] Garcia-Vidal F J, Martin-Moreno L, Ebbesen T W and Kuipers L 2010 Light passing through subwavelength apertures *Rev. Mod. Phys.* **82** 729–87

[3] Catrysse P B and Fan S 2007 Near-complete transmission through subwavelength hole arrays in phonon-polaritonic thin films *Phys. Rev.* B **75** 075422

[4] Chen Y-B, Huang M-J and Chen C-J 2012 Directional and hemispherical mid-infrared transmittance through microscale slit arrays on a semi-transparent substrate at normal incidence *J. Quant. Spectrosc. Radiat. Transfer* **113** 1951–60

[5] Lee B J, Chen Y B and Zhang Z M 2008 Confinement of infrared radiation to nanometer scales through metallic slit arrays *J. Quant. Spectrosc. Radiat. Transfer* **109** 608–19

[6] Shen H and Maes B 2012 Enhanced optical transmission through tapered metallic gratings *Appl. Phys. Lett.* **100** 241102

[7] Marquier F, Greffet J J, Collin S, Pardo F and Pelouard J L 2005 Resonant transmission through a metallic film due to coupled modes *Opt. Express* **13** 70–6

[8] Ye Y-H, Wang Z-B, Cao Y, Yan D, Zhang J-Y, Lin X Q and Cui T J 2007 Enhanced transmission through metal films perforated with circular and cross-dipole apertures *Appl. Phys. Lett.* **91** 251105

[9] Williams S M, Stafford A D, Rogers T M, Bishop S R and Coe J V 2004 Extraordinary infrared transmission of Cu-coated arrays with subwavelength apertures: hole size and the transition from surface plasmonto waveguide transmission *Appl. Phys. Lett.* **85** 1472–4

[10] Akarid A, Ourir A, Maurel A, Félix S and Mercier J-F 2014 Extraordinary transmission through subwavelength dielectric gratings in the microwave range *Opt. Lett.* **39** 3752–5

[11] van Beijnum F, Retif C, Smiet C B, Liu H, Lalanne P and van Exter M P 2012 Quasi-cylindrical wave contribution in experiments on extraordinary optical transmission *Nature* **492** 411–4

[12] Meng Z, Cheng-ping H, Guo-dong W and Yong-yuan Z 2010 Theory of extraordinary light transmission through sub-wavelength circular hole arrays *J. Opt.* **12** 015004

[13] Liu X L, Zhao B and Zhang Z M 2013 Wide-angle near infrared polarizer with extremely high extinction ratio *Opt. Express* **21** 10502–10

[14] Inoue D, Miura A, Nomura T, Fujikawa H, Sato K, Ikeda N, Tsuya D, Sugimoto Y and Koide Y 2011 Polarization independent visible color filter comprising an aluminum film with surface-plasmon enhanced transmission through a subwavelength array of holes *Appl. Phys. Lett.* **98** 093113

[15] Fan R-H, Peng R-W, Huang X-R, Li J, Liu Y, Hu Q, Wang M and Zhang X 2012 Transparent metals for ultrabroadband electromagnetic waves *Adv. Mater.* **24** 1980–6

[16] Gordon R, Sinton D, Kavanagh K L and Brolo A G 2008 A new generation of sensors based on extraordinary optical transmission *Acc. Chem. Res.* **41** 1049–57

[17] Tetz K A, Pang L and Fainman Y 2006 High-resolution surface plasmon resonance sensor based on linewidth-optimized nanohole array transmittance *Opt. Lett.* **31** 1528–30

[18] Coe J V, Heer J M, Teeters-Kennedy S, Tian H and Rodriguez K R 2008 Extraordinary transmission of metal films with arrays of subwavelength holes *Annu. Rev. Phys. Chem.* **59** 179–202

[19] Wang L P and Zhang Z M 2010 Effect of magnetic polaritons on the radiative properties of double-layer nanoslit arrays *J. Opt. Soc. Am.* B **27** 2595–604

[20] Chan H B *et al* 2006 Optical transmission through double-layer metallic subwavelength slit arrays *Opt. Lett.* **31** 516–8

[21] Cheng C, Chen J, Shi D J, Wu Q Y, Ren F F, Xu J, Fan Y X, Ding J P and Wang H T 2008 Physical mechanism of

extraordinary electromagnetic transmission in dual-metallic grating structures *Phys. Rev.* B **78** 075406

[22] Li W-D, Hu J and Chou S Y 2011 Extraordinary light transmission through opaque thin metal film with subwavelength holes blocked by metal disks *Opt. Express* **19** 21098–108

[23] Cui Y and He S 2009 Enhancing extraordinary transmission of light through a metallic nanoslit with a nanocavity antenna *Opt. Lett.* **34** 16–8

[24] García de Abajo F J 2014 Graphene plasmonics: challenges and opportunities *ACS Photonics* **1** 135–52

[25] Jablan M, Soljacic M and Buljan H 2013 Plasmons in graphene: fundamental properties and potential applications *Proc. IEEE* **101** 1689–704

[26] Hadiseh N and Mohammad S A 2014 Magnetically tunable focusing in a graded index planar lens based on graphene *J. Opt.* **16** 105502

[27] Low T and Avouris P 2014 Graphene plasmonics for terahertz to mid-infrared applications *ACS Nano* **8** 1086–101

[28] Liu X L, Zhang R Z and Zhang Z M 2014 Near-field radiative heat transfer with doped-silicon nanostructured metamaterials *Int. J. Heat Mass Transfer* **73** 389–98

[29] Ilic O, Jablan M, Joannopoulos J D, Celanovic I, Buljan H and Soljačić M 2012 Near-field thermal radiation transfer controlled by plasmons in graphene *Phys. Rev.* B **85** 155422

[30] Falkovsky L A 2008 Optical properties of graphene *J. Phys.: Conf. Ser.* **129** 012004

[31] Zhang Z M 2007 *Nano/Microscale Heat Transfer* (New York: McGraw-Hill)

[32] Zhao B, Wang L, Shuai Y and Zhang Z M 2013 Thermophotovoltaic emitters based on a two-dimensional grating/thin-film nanostructure *Int. J. Heat Mass Transfer* **67** 637–45

[33] http://zhang-nano.gatech.edu/

[34] Liu X L and Zhang Z M 2014 Graphene-assisted near-field radiative heat transfer between corrugated polar materials *Appl. Phys. Lett.* **104** 251911

[35] Vakil A and Engheta N 2011 Transformation optics using graphene *Science* **332** 1291–4

[36] Marques R, Mesa F, Martel J and Medina F 2003 Comparative analysis of edge- and broadside-coupled split ring resonators for metamaterial design—theory and experiments *IEEE Trans. Antennas Propag.* **51** 2572–81

[37] Baena J D *et al* 2005 Equivalent-circuit models for split-ring resonators and complementary split-ring resonators coupled to planar transmission lines *IEEE Trans. Microw. Theory Tech.* **53** 1451–61

[38] Zhao B and Zhang Z M 2014 Study of magnetic polaritons in deep gratings for thermal emission control *J. Quant. Spectrosc. Radiat. Transfer* **135** 81–9

[39] Wang L P and Zhang Z M 2009 Resonance transmission or absorption in deep gratings explained by magnetic polaritons *Appl. Phys. Lett.* **95** 111904

[40] Feng R, Qiu J, Cao Y, Liu L, Ding W and Chen L 2014 Omnidirectional and polarization insensitive nearly perfect absorber in one dimensional meta-structure *Appl. Phys. Lett.* **105** 181102

[41] Sakurai A, Zhao B and Zhang Z M 2014 Resonant frequency and bandwidth of metamaterial emitters and absorbers predicted by an rlc circuit model *J. Quant. Spectrosc. Radiat. Transfer* **149** 33–40

[42] Wang H, O'Dea K and Wang L 2014 Selective absorption of visible light in film-coupled nanoparticles by exciting magnetic resonance *Opt. Lett.* **39** 1457–60

[43] Xuan Y and Zhang Y 2014 Investigation on the physical mechanism of magnetic plasmons polaritons *J. Quant. Spectrosc. Radiat. Transfer* **132** 43–51

[44] Liu X L, Wang L P and Zhang Z M 2013 Wideband tunable omnidirectional infrared absorbers based on doped-silicon nanowire arrays *J. Heat Transfer* **135** 061602

[45] Liu X L, Zhang R Z and Zhang Z M 2014 Near-perfect photon tunneling by hybridizing graphene plasmons and hyperbolic modes *ACS Photonics* **1** 785–9

[46] Zhao B, Zhao J M and Zhang Z M 2014 Enhancement of near-infrared absorption in graphene with metal gratings *Appl. Phys. Lett.* **105** 031905

[47] Piper J R and Fan S 2014 Total absorption in a graphene monolayer in the optical regime by critical coupling with a photonic crystal guided resonance *ACS Photonics* **1** 347–53

[48] Lee B J, Wang L P and Zhang Z M 2008 Coherent thermal emission by excitation of magnetic polaritons between periodic strips and a metallic film *Opt. Express* **16** 11328–36

[49] Huang X-R, Peng R-W and Fan R-H 2010 Making metals transparent for white light by spoof surface plasmons *Phys. Rev. Lett.* **105** 243901

[50] Alu A, D'Aguanno G, Mattiucci N and Bloemer M J 2011 Plasmonic brewster angle: broadband extraordinary transmission through optical gratings *Phys. Rev. Lett.* **106** 123902

[51] Alonso-González P *et al* 2014 Controlling graphene plasmons with resonant metal antennas and spatial conductivity patterns *Science* **344** 1369–73

[52] Yao Y, Kats M A, Genevet P, Yu N, Song Y, Kong J and Capasso F 2013 Broad electrical tuning of graphene-loaded plasmonic antennas *Nano Lett.* **13** 1257–64

[53] Slipchenko T M, Nesterov M L, Martin-Moreno L and Nikitin A Y 2013 Analytical solution for the diffraction of an electromagnetic wave by a graphene grating *J. Opt.* **15** 114008

[54] Ju L, Geng B, Horng J, Girit C, Martin M, Hao Z, Bechtel H A, Liang X, Zettl A and Shen Y R 2011 graphene plasmonics for tunable terahertz metamaterials *Nat. Nanotechnology* **6** 630–4

[55] Feng R, Qiu J, Liu L, Ding W and Chen L 2014 Parallel LC circuit model for multi-band absorption and preliminary design of radiative cooling *Opt. Express* **22** A1713–24

[56] Chen Y B and Zhang Z M 2007 Design of tungsten complex gratings for thermophotovoltaic radiators *Opt. Commun.* **269** 411–7

[57] Wang H and Wang L 2013 Perfect selective metamaterial solar absorbers *Opt. Express* **21** A1078–93